Chemical Science

ROYAL SOCIETY OF CHEMISTRY

EDGE ARTICLE

View Article Online
View Journal

Cite this: DOI: 10.1039/d5sc10068b

All publication charges for this article have been paid for by the Royal Society of Chemistry

Rational design of a polyphenyl octacarboxylate HOF for highly selective separation of benzene over cyclohexane

Biying Liu,†[a] Ying Wang,†[b] Miao She,†[a] Tianfu Liu,[cd] Manxin Luo,[a] Yongxin Xie,[a] Defei Liu,[a] Ziyi Du,[a] Liyun Huang*[a] and Wenbing Yuan*[a]

The separation of benzene and cyclohexane is a long-standing challenge in the petrochemical industry, yet conventional distillation remains highly energy-intensive due to the nearly identical boiling points of the two molecules. Adsorptive separation offers a far more energy-efficient alternative; however, the development of adsorbents that simultaneously combine stable lightweight structures, high adsorption capacity, and strong selectivity remains difficult. To overcome these limitations, we present a robust hydrogen-bonded organic framework, H_8ETTOB-HOF, constructed from a polyphenyl octacarboxylic acid linker. Its precisely engineered pore architecture and tailored electrostatic environment work synergistically to enhance benzene affinity, affording exceptional benzene/cyclohexane selectivity (16.9) and a high adsorption capacity (3.9 mmol g^{-1} at 298 K, 13 kPa), surpassing all previously reported HOFs. Density functional theory shows that the synergistic C–H···O and C–H···π interactions facilitate benzene capture. Experimental investigations employing dynamic columns demonstrate efficient one-step benzene purification from equimolar mixtures, showcasing excellent recyclability. This work highlights a strategic approach to constructing stable, multifunctional HOFs for challenging hydrocarbon separations.

Received 23rd December 2025
Accepted 8th March 2026

DOI: 10.1039/d5sc10068b

rsc.li/chemical-science

1. Introduction

Cyclohexane (Cy) is an important petrochemical raw material and organic solvent that is mainly prepared by catalytic hydrogenation of benzene (Bz); however, the removal of Bz residues from the synthesis process in Cy is a challenge due to their similar boiling points (Bz, 80.1 °C; Cy, 80.7 °C), molecular size (Bz, 3.3 × 6.6 × 7.3 Å^3; Cy, 5.0 × 6.6 × 7.2 Å^3), kinetic diameters, *etc.* (Table S1).[1–3] The industrial separation of Bz/Cy mixtures currently relies primarily on energy-intensive extractive and azeotropic distillation methods, which involve complex processes and substantial operating costs.[4,5] While adsorptive separation represents a technologically superior alternative, its implementation hinges on the design of porous materials featuring essential characteristics: stability, light weight, high capacity, and exceptional selectivity.

Against this backdrop, both metal–organic frameworks (MOFs) and hydrogen-bonded organic frameworks (HOFs) have emerged as highly promising classes of materials. MOFs often achieve ultra-selective recognition of targeted molecules through precise pore engineering and functionalization,[6–8] such as JNU-81-C,[9] UiO-66/MFM-300 (ref. 10) and Zn-Ade-TCPE.[11] In contrast, HOFs possess distinct advantages due to their mild synthesis conditions, readily tunable pore structures, and inherent molecular recognition capabilities. HOFs are porous crystalline materials composed of molecular building blocks connected through intermolecular hydrogen bonds.[12–15] HOFs possess significant advantages such as light weight, high crystallinity, processability in solution, exceptional recyclability, and easy purification, endowing them with promising potential for gas adsorption and separation, proton conduction, drug delivery, and so on.[16,17] Recent advancements in HOFs have demonstrated their potential in the selective adsorption of aromatic compounds like benzene. For instance, HOF-8 displays a benzene uptake of ~2.5 mmol g^{-1} at 298 K, with its ordered π-stacked pores favoring aromatic adsorption *via* van der Waals and π···π interactions.[18] The B ← N-based framework of BNH-1 shows ~2.2 mmol g^{-1} toluene uptake and effectively separates it from methylcyclohexane, enabled by directional C–H···π interactions and a self-healing hydrogen-bonded network.[19] Nevertheless, achieving efficient discrimination between structurally similar aromatic and aliphatic molecules—such as benzene and cyclohexane—remains challenging for HOFs, due to limitations in pore rigidity, binding site definition, and framework persistence. These challenges

[a]*School of Environmental and Chemical Engineering, Foshan University, Foshan 528000, P. R. China. E-mail: huangliyun@fosu.edu.cn; hnyuanwb@126.com*

[b]*School of Environmental and Chemical Engineering, Wuyi University, Jiangmen 529020, P. R. China*

[c]*State Key Laboratory of Structural Chemistry, Fujian Institute of Research on the Structure of Matter, Chinese Academy of Sciences, Fuzhou 350002, P. R. China*

[d]*University of the Chinese Academy of Sciences, Beijing 100049, China*

† These authors equally contributed to this work.

underscore the need for rational design of HOFs featuring enhanced connectivity, shape-selective cavities, and stable hydrogen-bonded architectures to achieve high selectivity and structural robustness for aromatic-aliphatic separations.[20,21]

For HOFs, the well-known inherent weakness of hydrogen bonds often renders them fragile, making it challenging to sustain their permanent porosity, which significantly impedes the use of these materials. To date, considerable endeavors have been undertaken to construct stable HOFs with accessible permanent porosity.[22] Among them, increasing the number of connection sites in the building blocks improves connectivity and promotes interpenetration. This structural reinforcement contributes to greater framework robustness. Furthermore, strengthening the interlocking interactions between interpenetrating layers can further improve the chemical and thermal stability of HOFs. Moreover, the combination of rigid and flexible organic polycarboxylic acids can increase the connectivity of the constructed HOF, and it is also likely to increase the degree of interpenetration, which is a very effective way to improve the stability of HOFs. Currently, the vast majority of ligands in HOFs are at most six-linked. Bu *et al.* reported rare 8-connected carboxyl hydrogen-bonded organic frameworks, NKM–HOF–1 and NKM–HOF–2, for white light emission.[23] Generally, HOFs are "soft" and always in a balanced state of robustness and flexibility.[24] HOFs constructed from rigid and flexible organic compounds with more than six potential multi-linker sites happen to have this softness or flexibility, which increases the interpenetration degree, and their inherent pores have a more sensitive corresponding adaptability to the storage of guest molecules.

Thus, designing a new HOF should focus on organic polyphenyl linkers, multi-connectivity, and a rigid framework to maintain narrow windows, allowing for effective host-guest van der Waals interactions, especially with benzene over cyclohexane. Herein, we designed and synthesized a novel tetraphenylethylene (TPE)-based octacarboxylic HOF, designated as H_8ETTOB-HOF, constructed from 4,4′,4″,4‴,4⁗,4⁗′,4⁗″,4⁗‴–((ethene-1,2,2 tetrayltetrakis (benzene-4,1-diyl))tetrakis- (azanetriyl))octabenzoic acid (H_8ETTOB, Fig. 1a) as the molecular building block. This stable framework with π-conjugated aromatic linkers or aromatic pore surfaces can preferentially interact with aromatic guests compared to aliphatic ones. The judicious arrangement of these components facilitates stable assembly, exhibiting potential for selective adsorption and separation of Bz from Cy.

2. Results and discussion

The synthesis of the eight-connected carboxylic ligand H_8ETTOB was accomplished through a carefully controlled multi-step reaction sequence.[25] Single crystals of H_8ETTOB-HOF were obtained by slow evaporation of a tetrahydrofuran/acetone solution at room temperature. Single-crystal X-ray diffraction (SCXRD) revealed that H_8ETTOB-HOF crystallizes in the orthorhombic space group *Pbca*, with lattice parameters: $a = 43.850$ (5) Å, $b = 9.088$ (2) Å, $c = 44.605$ (7) Å, a unit cell volume of 17 776.3 (5) Å^3, and a density of 1011 g cm^{-3} at 100 K (Table S2). The H_8ETTOB framework is stabilized by eight carboxylic groups *via* O–H···O hydrogen bonds, forming a robust three-dimensional (3D) network.[26] The O–H···O bond lengths range

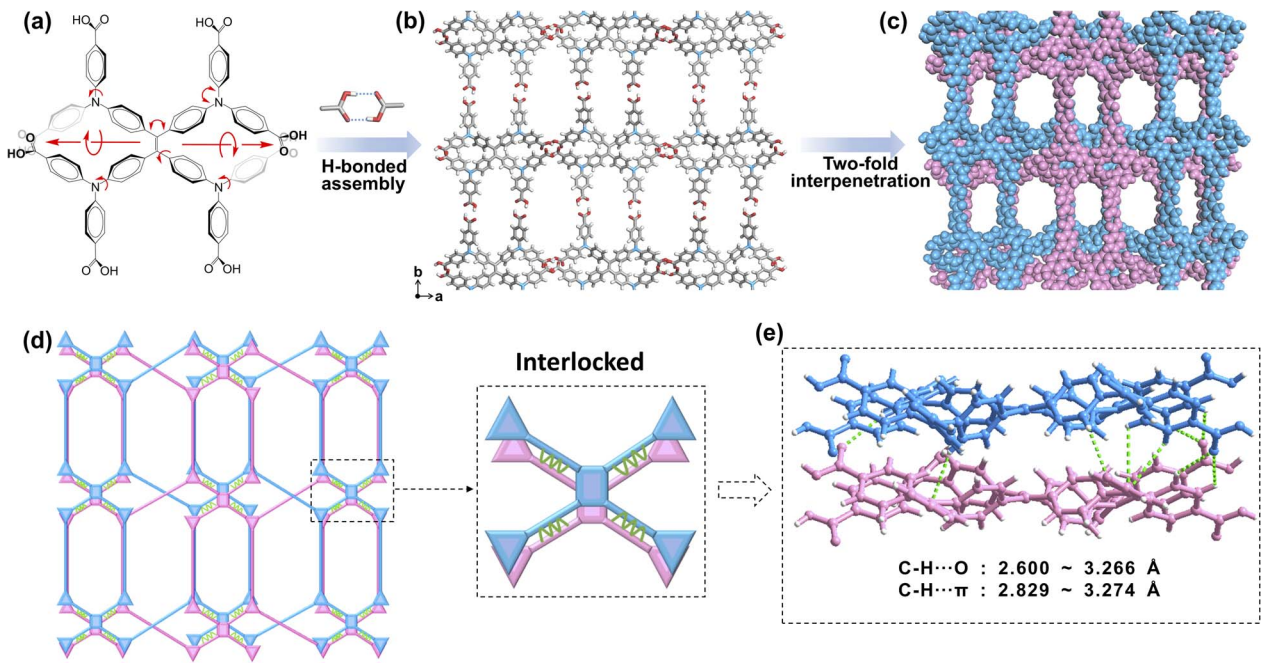

Fig. 1 Crystal structure of H_8ETTOB-HOF: (a) the chemical structure of the 8-c ligand exhibiting flexible and adaptable structural characteristics facilitated by bond rotation, the presence of a helical axis, and variations in bond angles; (b) the adjacent interlayer hydrogen bond connection mode , color code: C, gray; O, red; N, blue; H, white; (c) the extended structures of twofold interpenetrated H_8ETTOB-HOF along the *c* axis; (d) a simplified connectivity pattern in centrosymmetric *Pbca*, forming a symmetric center through interpenetration (simplifying the building blocks of 6-c into four 3-c units and one 4-c unit); (e) the interlocking interlayer interaction force.

from 2.586 to 2.653 Å with angles near 170°, indicating strong and directional hydrogen bonding. These values are consistent with reported data for similar HOFs (Fig. 1 and S3, Table S3).[27,28]

In this structure, adjacent layers are interconnected by additional O–H···O hydrogen bonds (2.601 Å – 2.699 Å), reinforcing the stability of the 3D framework (Fig. 1b, c and S3). The C37–H37···O12 and C56–H56···O4 interactions (3.455 Å and 3.400 Å, respectively, Table S3) further enhance the structural integrity.[29,30] These supramolecular interactions stabilize the framework while imparting flexibility due to their weak nature. Fig. 1d, e and S4 illustrate the hydrogen bonding interactions within and between layers, forming a robust 3D interlocked network. This structural arrangement, featuring intra- and inter-layer hydrogen bonds, generates stable yet flexible porosity, making H_8ETTOB-HOF promising for gas adsorption and separation.[31]

Notably, H_8ETTOB acts as a building block for H_8ETTOB-HOF, which exhibits an unexpected coordination number of six, forming unconventional "double link" connections (Fig. 1d, e and S4). For accurate topological analysis, we deconstructed each 8-c building block into one four-connected (4-c) vertex and four trigonal (3-c) vertices, revealing a 6-c topology (Fig. 1d).[32] The layers feature alternating large and small hexagonal structures. The slight misalignment between adjacent large hexagons creates zigzag channels, with a similar pattern observed in the smaller hexagons. This results in two distinct one-dimensional (1D) channels with window sizes of approximately 12 × 8 $Å^2$ and 9 × 6 $Å^2$ (Fig. S5), sufficiently large to accommodate Bz and Cy molecules (Table S1).

The network topology of H_8ETTOB-HOF, as analyzed by the ToposPro program, features fully interdigitated symmetry elements, classifying it as a twofold interpenetrated framework.[27,33] The framework exhibits a 6-connected net with the Schläfli symbol $4^{12}\cdot6^3$. As shown in Fig. S5, H_8ETTOB-HOF displays a pcu (primitive cubic) topology with alpha-Po-like charateristics, integrating the geometric features of both nets, which likely endows the material with distinctive physicochemical properties. The H_8ETTOB building block exhibits flexible and adaptable structural characteristics facilitated by bond rotation, the presence of a helical axis (Fig. 1a), and variations in bond angles, to form a stable and functional framework. The single-layer structure of H_8ETTOB-HOF is connected by hydrogen bonds, displaying a "double-spiral upward figure-eight" pattern along the *b*-axis (Fig. S6). Correspondingly, two layers of these "spiral eight-shaped chains" of H_8ETTOB-HOF become intertwined and risen. These robust interlayer hydrogen bonding interactions and the structural feature of two helices, combined with the well-defined porous channels, contribute to the stability and functionality of the 3D framework of H_8ETTOB-HOF.

The powder X-ray diffraction (PXRD) patterns of H_8ETTOB-HOF were carefully examined under various conditions, including as-synthesized and thermally activated (473 K) (Fig. 2a). The experimental patterns match well with the simulated one, confirming framework integrity upon thermal treatment. To evaluate chemical stability, H_8ETTOB-HOF was immersed in concentrated hydrochloric acid (12 M), NaOH aqueous solution (pH = 11), H_2O, methanol, ethyl acetate, and acetone for 3 days, and PXRD showed that H_8ETTOB-HOF maintained its crystallinity (Fig. 2a and S7c). Optical microscopy and scanning electron microscopy (SEM) results show that the crystal form does not change under various soaking conditions (Fig. S1 and S2). These observations demonstrate that H_8ETTOB-HOF maintains its morphological integrity under chemically aggressive conditions. Furthermore, thermal stability was investigated using variable-temperature X-ray diffraction (VT-XRD): the diffraction patterns remain consistent from 298 K to 473 K, confirming that the crystal structure of H_8ETTOB-HOF is stable up to high temperatures (Fig. S7d). Complementary FTIR spectra (Fig. S7a) reinforce the stability of the framework, with strong absorption bands in the –COOH region (1700–1500 cm^{-1}) affirming the integrity of carboxylic groups within the HOF. Notably, the TGA curves (Fig. S7b) for both untreated and post-activation H_8ETTOB-HOF reveal comparable weight loss patterns, with significant decomposition commencing around 573 K, attributed to the breakdown of organic ligands. Compared to similar hexacarboxylic acid-based HOFs reported in the literature,[34] H_8ETTOB-HOF exhibits superior thermal stability, likely due to its high connectivity and robust framework.[25] Additionally, nitrogen adsorption–

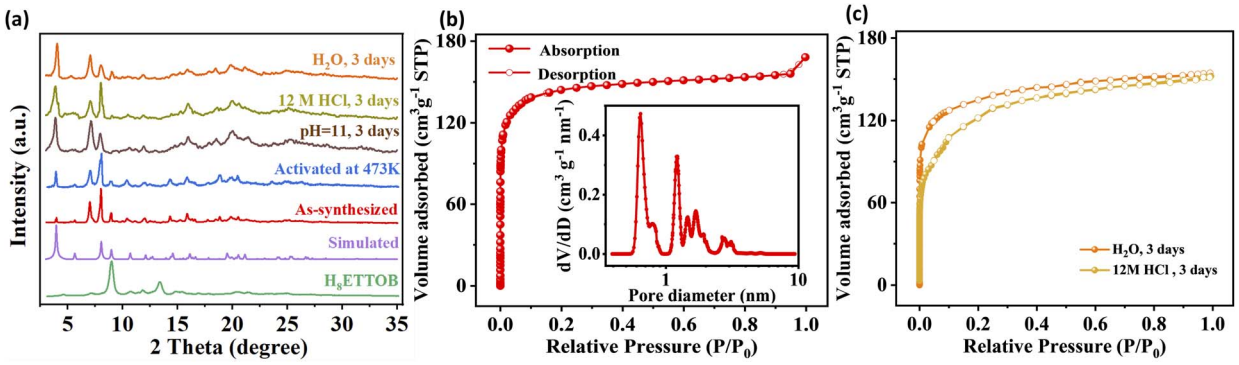

Fig. 2 (a) PXRD of H_8ETTOB, and simulated, synthesized and treated H_8ETTOB-HOF. (b) N_2 adsorption isotherms of H_8ETTOB-HOF at 77 K. (inset: the pore size distribution was calculated using non-local density functional theory (NLDFT)). (c) N_2 adsorption isotherms (at 77 K) of H_8ETTOB-HOF immersed in concentrated hydrochloric acid (12 M) and H_2O for 3 days, respectively.

desorption isotherms (Fig. 2b) of H_8ETTOB-HOF activated at 473 K reveal a Brunauer–Emmett–Teller (BET) surface area of 555.11 $m^2\ g^{-1}$ and a pore volume of 0.26 $cm^3\ g^{-1}$. Nonlocal density functional theory (NLDFT) pore size distribution indicated a main pore at 6.4 Å, with additional pores distributed in the range of 12.0 to 18.5 Å (Fig. 2b). Notably, the H_8ETTOB-HOF exhibits remarkable chemical stability, as evidenced by its BET surface areas (Fig. 2c) of 509.18 and 453.73 $m^2\ g^{-1}$ after immersion in concentrated hydrochloric acid (12 M) and water for 3 days, respectively. These results are consistent with the PXRD data, further confirming the structural integrity of H_8ETTOB-HOF under harsh conditions.

The demonstration of permanent porosity in H_8ETTOB-HOF promoted an investigation into the single-component adsorption isotherms of Bz and Cy at 298, 318, and 373 K, at pressures up to 13 kPa. As shown in Fig. 3a, S6a and S7, H_8ETTOB-HOF exhibits a pronounced preference for Bz over Cy at all tested temperatures. At 298 K and 13 kPa, the Bz uptake reaches 3.9 mmol g^{-1}, significantly higher than that of Cy (1.2 mmol g^{-1}), resulting in a high Bz/Cy uptake ratio. Ideal adsorbed solution theory (IAST) was applied to calculate the adsorption selectivity of H_8ETTOB-HOF towards binary Bz/Cy mixtures (50 : 50, v/v) at 298, 318, and 373 K. As shown in Fig. 3b and S9, the IAST selectivity of H_8ETTOB-HOF for benzene over cyclohexane exhibits a notable pressure-dependent increase at various temperatures. At 298 K, the selectivity reached 16.9 at 14 kPa, underscoring its pronounced affinity for benzene under ambient conditions. As the temperature increased, the selectivity decreased to approximately 10 at 318 K, indicating that elevated thermal energy reduced the differential adsorption affinity between benzene and cyclohexane. Subsequently, the selectivity rose significantly to 20 at 373 K. This recovery is attributed to a pronounced thermal contraction of the HOF pore apertures, which imposes a stronger steric restriction on the bulkier cyclohexane molecule.[35] In contrast, the planar benzene molecule maintains efficient adsorption through resilient π–π interactions with the aromatic pore walls, thereby preserving high separation efficacy even at elevated temperature interactions.[36] The nearly linear progression of selectivity with pressure at each temperature suggests a stable adsorption behavior, maintaining significant Bz/Cy discrimination even at elevated pressures. The PXRD patterns confirm the structural stability of H_8ETTOB-HOF after Bz/Cy uptake (Fig. S8a).

The adsorption heat (Q_{st}) for Bz was calculated to be approximately 42 kJ mol^{-1} at zero coverage, higher than that for Cy (~30 kJ mol^{-1}), indicating stronger interactions with Bz (Fig. 3c and S11).[37,38] Additionally, the gentle upward trend in the Q_{st} curve over a broad range of adsorbed amounts suggests additional intermolecular interactions as gas molecules progressively stack within the pore channels until saturation.[39] The exceptional performance of H_8ETTOB-HOF in Bz capture is attributed to its fine-tuned pore structure, the polyphenyl environment of its pore walls, and its strong binding affinity for Bz molecules. The adsorption isotherms of benzene in H_8ETTOB-HOF display a distinct profile, indicating strong interactions and efficient accommodation within the framework's channels (Fig. S10). Notably, the adsorption data were effectively modelled using the dual-site Langmuir–Freundlich

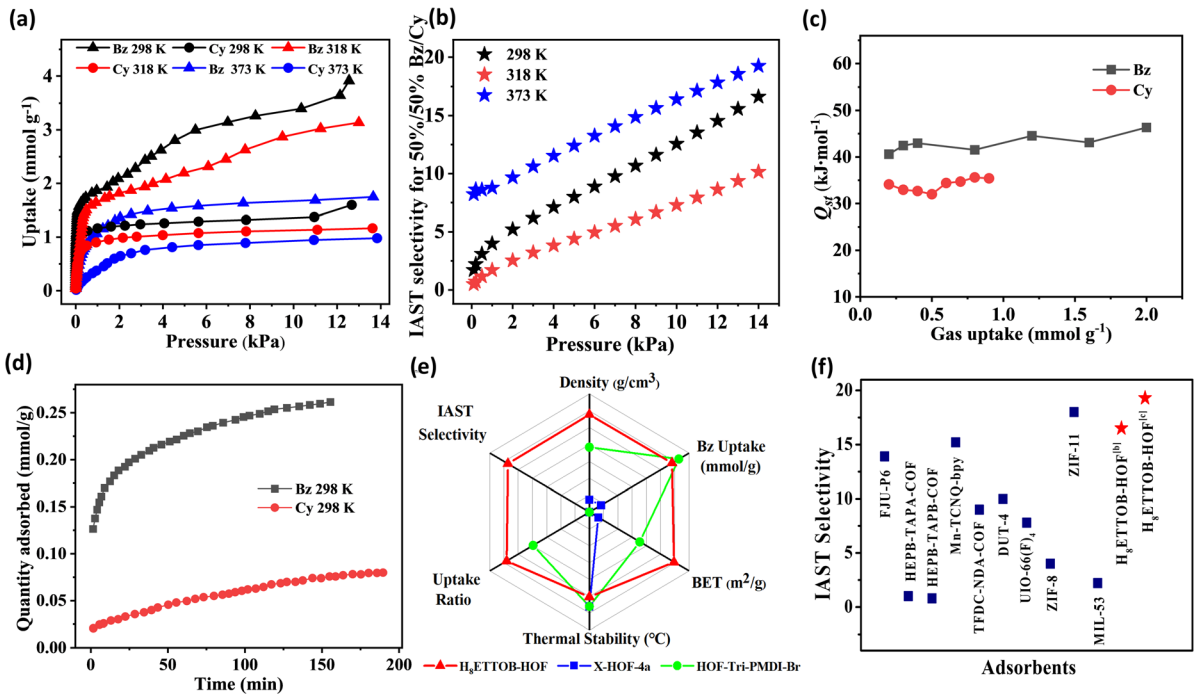

Fig. 3 (a) Adsorption isotherms of Bz and Cy on H_8ETTOB-HOF at 298 K, 318 K and 373 K; (b) IAST selectivity of H_8ETTOB-HOF for 50/50 Bz/Cy at different temperatures. (c) Isosteric heat of adsorption (Qst) plots for the adsorption of Bz and Cy by H_8ETTOB-HOF. (d) Adsorption kinetic curves of Bz and Cy on H_8ETTOB-HOF at 298 K under 200 Pa. (e) Trends in performance for the HOFs.[45,46] (f) Performance comparison of IAST selectivity between H_8ETTOB-HOF and classical adsorbents.[47–52]

(DSL-F) fitting, which revealed the presence of two types of adsorption sites within the H_8ETTOB-HOF framework. The high-affinity sites, as indicated by the Langmuir model, suggest strong and uniform adsorption, likely driven by π–π interactions and hydrogen bonding with benzene.[40] In contrast, the low-affinity sites, modelled by the Freundlich approach, are indicative of a more heterogeneous surface, supporting multilayer adsorption and weaker van der Waals interactions, which are more characteristic of cyclohexane.[41] This dual-site nature elucidates the observed higher selectivity and uptake of benzene, particularly at lower temperatures and higher pressures.

To further elucidate the adsorption kinetics of benzene Bz and Cy within H_8ETTOB-HOF, we measured the kinetic adsorption curves at 298 K and 200 Pa. As depicted in Fig. 3d, Bz reached adsorption equilibrium in approximately 160 min, whereas Cy required around 190 min to do so. The diffusion time constant (D/r^2), obtained from the short-time approximation of the diffusion equation,[42] reveals a kinetic selectivity of 21.4 for Bz/Cy in the H_8ETTOB-HOF (Fig. S12 and Table S5–S6). The significantly higher value implies a greater relative diffusivity of Bz compared to Cy, likely attributable to the size-exclusion effect imposed by the pore channels on the bulkier Cy molecules.[43] The faster adsorption rate of Bz compared to Cy suggests a more rapid intra-crystalline diffusion for Bz, indicating a higher affinity and interaction with the framework of H_8ETTOB-HOF.[44] Fig. 3e presents a radar chart comparison of key performance indicators—including IAST selectivity, Bz uptake, BET surface area, uptake ratio, density, and thermal stability—among H_8ETTOB-HOF and representative HOF analogs such as X–HOF–4a[45] and HOF-Tri-PMDI-Br.[46] H_8ETTOB-HOF demonstrates a balanced profile, with notably higher Bz uptake and IAST selectivity, indicating its superior adsorption capacity and affinity toward aromatic molecules under ambient conditions. Fig. 3f presents a comparative analysis of IAST selectivity for Bz over Cy across various porous materials. H_8ETTOB-HOF exhibits a notably higher selectivity (16.9) than most classical COFs and MOFs. This highlights its superior molecular recognition capability among metal-free frameworks.

To verify the selective adsorption capabilities of H_8ETTOB-HOF in mixed Bz/Cy, we conducted column breakthrough experiments at 298 K using a 50 : 50 Bz/Cy mixture. At a flow rate of 0.6 mL min^{-1}, the breakthrough curve shows that Cy was eluted from the column first at 59.4 $min \cdot g^{-1}$, while Bz began to penetrate the column at 112.8 $min \cdot g^{-1}$, with a time interval of 53.4 $min \cdot g^{-1}$. This indicates that H_8ETTOB-HOF has a higher selectivity for Bz than for Cy (Fig. 4a). At a flow rate of 1.2 mL min^{-1} for the Bz/Cy mixture, the separation factor of 3.35 (eqn (S6)) outperforms HOF-FJU-112a (2.28),[36] HOF-202 (2.79)[53] and HOF-303 (2.95).[54] Moreover, as the flow rate increased from 0.6 to 0.9 and 1.2 mL min^{-1}, the retention time of Bz on the H_8ETTOB-HOF column gradually decreased from 53.4 to 43.6 and 28.9 $min \cdot g^{-1}$. The adsorption capacity of the material remained stable at approximately 3.1–3.6 mmol g^{-1} during three consecutive regeneration cycles under a flow rate of 1.2 mL min^{-1} (Fig. 4b and c), which further confirmed the stability of H_8ETTOB-HOF. Besides, the samples after three penetration cycles still maintained consistency with the PXRD, FT-IR and 77 K N_2 adsorption curves of the pristine samples, indicating that the samples were stable (Fig. S7a and S8).

To gain a deeper understanding of the selective adsorption behavior in H_8ETTOB-HOF, density functional theory (DFT) calculations were employed to analyze the energy profiles and molecular interactions of Bz and Cy. The electrostatic potential (ESP) analysis of H_8ETTOB-HOF, Bz, and Cy molecules reveals that the positive ESP on Bz's H atoms complements the negative ESP along H_8ETTOB-HOF's pore channels (Fig. 5a and b).[55] This electrostatic synergy drives the selective adsorption of Bz. Fig. 5c, d and S13 further show that Bz forms C–H···π interactions (2.99 Å) and C–H···O interactions (2.21 to 3.12 Å) with H_8ETTOB-HOF, whereas Cy exhibits only C–H···O interactions (2.61 to 3.08 Å). The binding energy of Bz (−79 kJ mol^{-1}) is higher than that of Cy (−62 kJ mol^{-1}).[56]

The energy variations as Bz and Cy traverse different adsorption sites—transitioning from the initial state (IS) through the transition state (TS) to the final state (FS)—are depicted in Fig. 5e and S14. The lower TS energy of Bz (12.7 *vs.* 21.2 kJ mol^{-1}) indicates its thermodynamic preference in H_8ETTOB-HOF. Further analysis of the energy landscapes for Bz

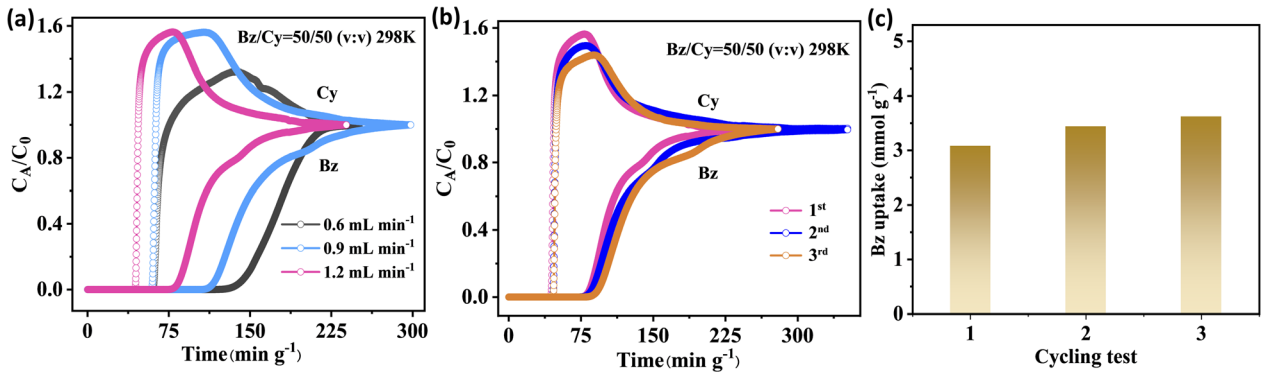

Fig. 4 Dynamic column breakthrough evaluation of H_8ETTOB-HOF for Bz/Cy separation. (a) Breakthrough profiles under different feed flow rates (0.6, 0.9, and 1.2 mL min^{-1}). (b) Three consecutive breakthrough cycles at a flow rate of 1.2 mL min^{-1}. (c) Corresponding Bz adsorption capacities for each cycle in (b).

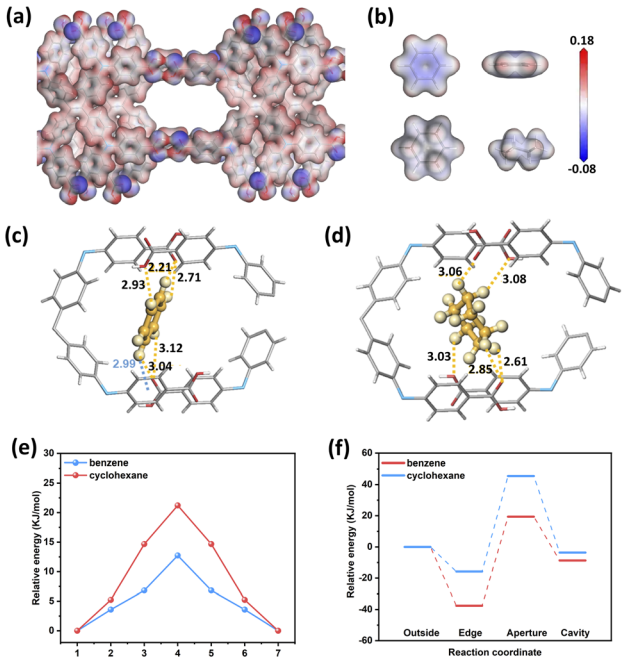

Fig. 5 Adsorption and energy profiles of Bz and Cy in H_8ETTOB-HOF. The electrostatic potential (ESP) of (a) H_8ETTOB-HOF and (b) Bz and Cy. The adsorption binding model of (c) Bz and (d) Cy within the H_8ETTOB-HOF framework, respectively. (e) Relative energy profiles of Bz and Cy along the reaction coordinate. (f) Relative energy changes of Bz and Cy at various positions within H_8ETTOB-HOF.

and Cy adsorption across different sites-outside, edge, aperture, and cavity—is presented in Fig. 5f. Bz exhibits relative energies of −37.6 kJ mol^{-1} (edge), −19.4 kJ mol^{-1} (aperture), and −8.7 kJ mol^{-1} (cavity), wheares Cy shows weaker relative energies: −15.8 kJ mol^{-1} (edge), 45.5 kJ mol^{-1} (aperture), and −3.6 kJ mol^{-1} (cavity). This stark contrast underscores Bz's superior affinity.[57,58] The energy differences are attributed to the structural properties of Bz and Cy: Bz's planar and aromatic structure facilitates C–H···π and C–H···O interactions with the framework, enhancing its adsorption stability.[59,60]

3 Conclusions

In summary, we developed a novel hydrogen-bonded organic framework, H_8ETTOB-HOF, characterized by optimal pore sizes and functional sites that exhibit marked preferential adsorption of Bz over Cy. Our results demonstrate that H_8ETTOB-HOF not only possesses exceptional chemical and thermal stability but also outperforms most reported Bz-selective HOFs in separation performance. Specifically, H_8ETTOB-HOF exhibits a high Bz uptake of 3.9 mmol g^{-1} at 298 K, and achieves a remarkable Bz/Cy selectivity of 16.9 among known HOFs. Breakthrough experiments confirm its ability to directly produce high-purity Cy from Bz/Cy mixtures. DFT calculations reveal that the Bz adsorption is energetically favored due to stronger C–H···π and C–H···O interactions compared to Cy. This study not only enhances the understanding of HOF self-assembly and structural transformation mechanisms, but also demonstrates H_8ETTOB-HOF's potential in industrial separation processes.

Author contributions

B. Liu and M. She conceived, designed, and performed the experiments. Y. Wang performed the density functional theory (DFT) calculations, designed the experiments and supervised the completion of the manuscript. T. Liu, Y. Xie, M. Luo, D. Liu, and Z. Du participated in the discussions. W. Yuan and L. Huang conceptualized the topic and structure of the paper, and outlined, drafted, and supervised the completion of the manuscript. All authors contributed to data interpretation and manuscript revision, and approved the final version.

Conflicts of interest

There are no conflicts to declare.

Data availability

The data supporting this article have been included as part of the supplementary information (SI). Supplementary information: The supplementary information includes all synthetic procedures, characterization data, spectral data, additional figures, and detailed information. See DOI: https://doi.org/10.1039/d5sc10068b.

Acknowledgements

This work was supported by the Guangdong Basic and Applied Basic Research Foundation (project ref. 2022A1515140170, 2022A1515140088), Foshan Engineering and Technology Research Center for Novel Porous Materials, and Foshan Zhibao Ecological Technology Co., Ltd (project reference: KH23155), for their financial support.

Notes and references

1 G.-A. Li, M. Deng, W. Guo, S. Yin, Y.-E. Liu, A.-X. Zhu and M. J. Zaworotko, *Inorg. Chem. Front.*, 2025, **12**, 3449–3455.
2 S. Mukherjee, D. Sensharma, O. T. Qazvini, S. Dutta, L. K. Macreadie, S. K. Ghosh and R. Babarao, *Coord. Chem. Rev.*, 2021, **437**, 213852.
3 Z. Zhang, S. B. Peh, C. Kang, K. Chai and D. Zhao, *EnergyChem*, 2021, **3**, 100057.
4 J. Qin, Q. Ye, X. Xiong and N. Li, *Ind. Eng. Chem. Res.*, 2013, **52**, 10754–10766.
5 M. Ayuso, A. Cañada-Barcala, M. Larriba, P. Navarro, N. Delgado-Mellado, J. García and F. Rodríguez, *Sep. Purif. Technol.*, 2020, **240**, 116583.
6 Y. He, S. Xiang and B. Chen, *J. Am. Chem. Soc.*, 2011, **133**, 14570–14573.
7 W. Liu and H. Zhang, *Angew. Chem., Int. Ed.*, 2025, **64**, e202418654.
8 D.-D. Zhou, Y. Liu and J. Zhang, *J. Am. Chem. Soc.*, 2025, **147**, 4035–4044.
9 Z. J. Jiang, Y. Wang, W. Lu and D. Li, *J. Am. Chem. Soc.*, 2025, **147**, 580144.

10 X.-J. Xie, H. Zeng, W.-G. Lu and D. Li, *Chem*, 2024, **11**, 1023–1038.
11 S. Yang and M. Schröder, *Chem*, 2025, **11**, 897–912.
12 R. Zhao, L. Xie and J. Li, *J. Am. Chem. Soc.*, 2024, **146**, 48921–48932.
13 Z.-J. Lin and R. Cao, *Acta Chim. Sin.*, 2020, **78**, 1309.
14 M. Zhao, L. Sun, Y. Yang, X.-S. Gu and C.-J.-S. Lai, *Coord. Chem. Rev.*, 2024, **514**, 215881.
15 Y. Suzuki and I. Hisaki, *Polym. J.*, 2024, **56**, 1–16.
16 A. Ebadi Amooghin, H. Sanaeepur, M. Ghomi, R. Luque, H. Garcia and B. Chen, *Coord. Chem. Rev.*, 2024, **505**, 215660.
17 Y.-L. Li, E. V. Alexandrov, Q. Yin, L. Li, Z.-B. Fang, W. Yuan, D. M. Proserpio and T.-F. Liu, *J. Am. Chem. Soc.*, 2020, **142**, 7218–7224.
18 X.-Z. Luo, X.-J. Jia, J.-H. Deng, J.-L. Zhong, H.-J. Liu, K.-J. Wang and D.-C. Zhong, *J. Am. Chem. Soc.*, 2013, **135**, 11684–11687.
19 Y. Li, H. Chen, J. Huang, H. Zhang, S. Lin, Z.-M. Ye, S. Xiang, B. Chen and Z. Zhang, *J. Am. Chem. Soc.*, 2024, **146**, 19425–19433.
20 Q. Huang, W. Li, Z. Mao, L. Qu, Y. Li, H. Zhang, T. Yu, Z. Yang, J. Zhao, Y. Zhang, M. P. Aldred and Z. Chi, *Nat. Commun.*, 2019, **10**, 3074.
21 X. Liu, G. Liu, T. Fu, K. Ding, J. Guo, Z. Wang, W. Xia and H. Shangguan, *Adv. Sci.*, 2024, **11**, 2400101.
22 X. Song, Y. Wang, C. Wang, D. Wang, G. Zhuang, K. O. Kirlikovali, P. Li and O. K. Farha, *J. Am. Chem. Soc.*, 2022, **144**, 10663–10687.
23 X.-J. Xi, Y. Li, F. Lang, J. Pang and X.-H. Bu, *Chem. Sci.*, 2024, **15**, 4529–4537.
24 J. P. Garcia Villaluenga and A. Tabe-Mohammadi, *J. Membr. Sci.*, 2000, **169**, 159–174.
25 X. Deng, M. Deng, Y.-L. Li, Z. Liu, T.-F. Liu, X. Chen, S. Cai, B. Liu, J. Li, D. Lv, J. Li and W. Yuan, *Chem. Eng. J.*, 2023, **474**, 145694.
26 K. Shao, H.-M. Wen, C.-C. Liang, X. Xiao, X.-W. Gu, B. Chen, G. Qian and B. Li, *Angew. Chem., Int. Ed.*, 2022, **61**, e202211523.
27 C.-H. Liu, L. Chen, H. Zhang, Y. Li, H. Lin, L. Li, J. Wu, C. Liu, Z.-M. Ye, S. Xiang, B. Chen and Z. Zhang, *Chem*, 2023, **9**, 3532–3543.
28 K. Adil, Y. Belmabkhout, R. S. Pillai, A. Cadiau, P. M. Bhatt, A. H. Assen, G. Maurin and M. Eddaoudi, *Chem. Soc. Rev.*, 2017, **46**, 3402–3430.
29 P. Li, Y. He, J. Guang, L. Weng, J. C.-G. Zhao, S. Xiang and B. Chen, *J. Am. Chem. Soc.*, 2014, **136**, 547–549.
30 B. Wang, R. He, L.-H. Xie, Z.-J. Lin, X. Zhang, J. Wang, H. Huang, Z. Zhang, K. S. Schanze, J. Zhang, S. Xiang and B. Chen, *J. Am. Chem. Soc.*, 2020, **142**, 12478–12485.
31 S. Feng, Y. Shang, Z. Wang, Z. Kang, R. Wang, J. Jiang, L. Fan, W. Fan, Z. Liu, G. Kong, Y. Feng, S. Hu, H. Guo and D. Sun, *Angew. Chem., Int. Ed.*, 2020, **59**, 3750.
32 J. Chang, Z. Zhang, H. Zheng, H. Li, J. Suo, C. Ji, F. Chen, S. Zhang, Z. Wang, V. Valtchev, S. Qiu, J. Sun and Q. Fang, *Nat. Chem.*, 2025, **17**, 571–581.
33 Q. Yin, E. V. Alexandrov, D.-H. Si, Q.-Q. Huang, Z.-B. Fang, Y. Zhang, A.-A. Zhang, W.-K. Qin, Y.-L. Li, T.-F. Liu and D. M. Proserpio, *Angew. Chem., Int. Ed.*, 2022, **134**, e202115854.
34 M. R. di Nunzio, Y. Suzuki, I. Hisaki and A. Douhal, *Int. J. Mol. Sci.*, 2022, **23**, 1929.
35 F. Xie, L. Chen, E. M. C. Morales, S. Ullah, Y. Fu, T. Thonhauser, K. Tan, Z. Bao and J. Li, *Nature*, 2024, **15**, 2345.
36 W. Wei, Y. Li, F. Yuan, Y. Lin, H. Lin, G. Han, B. Ma, Z. Yuan, S. Xiang, B. Chen and Z. Zhang, *Angew. Chem., Int. Ed.*, 2026, **65**, e19313.
37 S.-M. Wang, M. Shivanna and Q.-Y. Yang, *Angew. Chem., Int. Ed.*, 2022, **61**, e202201017.
38 Q. Zhang, L. Zhou, P. Liu, L. Li, S.-Q. Yang, Z.-F. Li and T.-L. Hu, *Sep. Purif. Technol.*, 2022, **296**, 121404.
39 Y. Cai, J. Gao, J.-H. Li, P. Liu, Y. Zheng, W. Zhou, H. Wu, L. Li, R.-B. Lin and B. Chen, *Angew. Chem., Int. Ed.*, 2023, **135**, e202308579.
40 D.-D. Zhou, X. Feng, D.-Y. Hu, X.-T. Lu, F.-D. Dong, Z.-L. Fang, R.-B. Lin, J.-P. Zhang and X.-M. Chen, *J. Am. Chem. Soc.*, 2025, jacs.5c03564.
41 M. Wasilewska, A. Derylo-Marczewska and A. W. Marczewski, *Molecules*, 2024, **29**, 2038.
42 J. Chang, F. Chen, H. Li, J. Suo, H. Zheng, J. Zhang, Z. Wang, L. Zhu, V. Valtchev, S. Qiu and Q. Fang, *Nature*, 2024, **15**, 813.
43 J. Cui, Z. Zhang, L. Yang, J. Hu, A. Jin, Z. Yang, Y. Zhao, B. Meng, Y. Zhou, J. Wang, Y. Su, J. Wang, X. Cui and H. Xing, *Science*, 2024, **383**, 179–183.
44 Y. Han, Y. Chen, Y. Ma, J. Bailey, Z. Wang, D. Lee, A. M. Sheveleva, F. Tuna, E. J. L. McInnes, M. D. Frogley, S. J. Day, S. P. Thompson, B. F. Spencer, M. Nikiel, P. Manuel, D. Crawshaw, M. Schröder and S. Yang, *Chem*, 2023, **9**, 739–754.
45 M. Liang, S. Hu, N. Zhou, Z. Liu, Q. Chen, X. Chen, X. Liu, C.-P. Li, J. Hao and P. Xue, *Small*, 2023, **19**, 2304340.
46 D. Wang and Y. Zhao, *Angew. Chem., Int. Ed.*, 2023, **135**(13), e202217903.
47 C. Jansen, N. Assahub, A. Spiess, J. Liang, A. Schmitz, S. H. Xing, S. Gökpinar and C. Janiak, *Nanomaterials*, 2022, **12**, 3614.
48 C. González-Galán, R. M. Madero-Castro, A. Luna-Triguero, J. M. Vicent-Luna and S. Calero, *Sep. Purif. Technol.*, 2024, **348**, 127606.
49 S. Shimomura, R. Matsuda and S. Kitagawa, *Chem. Mater.*, 2010, **22**, 4129.
50 L. Chen, H. Zhang, Y. Ye, Z. Yuan, J. Wang, Y. Yang, S. Lin, F. Xiang, S. Xiang and Z. Zhang, *New J. Chem.*, 2021, **45**, 22437.
51 P. Das and S. K. Mandal, *J. Mater. Chem. A*, 2018, **6**, 16246.
52 B. Cai, W. Wu, X. Miao, X. Yang, L. Duan, D. Lin and K. Yang, *Small*, 2024, 2408742.
53 L. Wang, H. Zhang, J. Li, Q. Liu and Y. Chen, *Ind. Eng. Chem. Res.*, 2024, **63**, 143678–143687.
54 F. Li, Z. Zhang, H. Guo and S. Wang, *Ind. Eng. Chem. Res.*, 2023, **62**, 112543–112552.
55 F. Yuan, G. Han, Y. Li, W. Wei, L. He, Y. Chen, C. Chen, G. Lan, S. Xiang, B. Chen and Z. Zhang, *Angew. Chem., Int. Ed.*, 2025, **64**, e202513288.

56 Y. Han, Y. Chen, Y. Ma, J. Bailey, Z. Wang, D. Lee, A. M. Sheveleva, F. Tuna, E. J. McInnes, M. D. Frogley and S. J. Day, *Chem*, 2023, **9**, 739–754.
57 B. Wang, R. He, L. H. Xie, Z.-J. Lin, X. Zhang, J. Wang, H. Huang, Z. Zhang, K. S. Schanze, J. Zhang, S. Xiang and B. Chen, *J. Am. Chem. Soc.*, 2020, **142**, 12478–12485.
58 L. Zhang, K. Jiang, L. Yang, L. Li, E. Hu, L. Yang, K. Shao, H. Xing, Y. Cui, Y. Yang, B. Li, B. Chen and G. Qian, *Angew. Chem., Int. Ed.*, 2021, **60**, 15995–16002.
59 J. P. Perdew, K. Burke and M. Ernzerhof, *Phys. Rev. Lett.*, 1996, **77**, 3865–3868.
60 S. Kandambeth, K. Dey and R. Banerjee, *J. Am. Chem. Soc.*, 2019, **141**, 1807–1822.